electronics

Article

Beampattern Synthesis and Optimization for Frequency Diverse Arc Array Based on the Virtual Element

Wei Xu [1,2,*], Zhuo Deng [1,2], Pingping Huang [1,2], Weixian Tan [1,2] and Zhiqi Gao [1,2]

1 College of Information Engineering, Inner Mongolia University of Technology, Hohhot 010051, China; 20201800089@imut.edu.cn (Z.D.); hwangpp@imut.edu.cn (P.H.); wxtan@imut.edu.cn (W.T.); gzqnd@163.com (Z.G.)
2 Inner Mongolia Key Laboratory of Radar Technology and Application, Hohhot 010051, China
* Correspondence: xuwei1983@imut.edu.cn; Tel.: +86-1581-159-7439

Abstract: With its special, arch-shaped array structure, a frequency diverse arc array (FDAA) can perform beam scanning in 360 degrees in azimuth and in arbitrary ranges by selectively activating array elements in different positions, utilizing array element phase compensation, and adopting a frequency offset design. In this paper, a beampattern synthesis and optimization method for FDDA using the virtual array element based on the geometric configuration of FDDA is proposed. First, the position of the virtual array element is determined by the direction of the target, and then activated array elements are selected. Afterwards, the frequency offset of each array element is set up on the equiphase surface to obtain the dot-shaped beampattern. Finally, amplitude weighting is introduced to suppress the increased sidelobe level of the dot-shaped beampattern, which is caused by inverse density weighting of the arch-shaped array structure. Simulation results validate the proposed method for beampattern synthesis and optimization in FDAA.

Keywords: frequency diverse arc array (FDAA); virtual array element; beampattern synthesis; sidelobe suppression

check for updates

Citation: Xu, W.; Deng, Z.; Huang, P.; Tan, W.; Gao, Z. Beampattern Synthesis and Optimization for Frequency Diverse Arc Array Based on the Virtual Element. *Electronics* **2023**, *12*, 2231. https://doi.org/10.3390/electronics12102231

Academic Editor: Reza K. Amineh

Received: 6 April 2023
Revised: 6 May 2023
Accepted: 12 May 2023
Published: 14 May 2023

1. Introduction

Frequency diverse array (FDA) radar was first proposed in 2006 as a system radar with a high degree of freedom [1]. Compared with a conventional phased array radar [2], FDA has a small frequency offset between radar antenna elements, so the phase superposition relationship of the transmitted signal in the far field changes with the target range, forming a beampattern related to range, angle, and time. FDA has time variations within each pulse and possesses flexible beam scanning characteristics [3,4]. Therefore, FDA has a wide range of applications, such as in the fields of target localization [5–7] and interference suppression [8–10].

FDA has been receiving increasing attention due to its unique range and angular spatial focusing properties [11–14]. To optimize the FDA dot-shaped beampattern, range-angle coupling in the FDA beampattern can be removed by using nonlinear array element spacing to break the periodicity of FDA [15] and by using a logarithmically increasing frequency offset [16]. The performance of the transmitted energy that is focused by increasing the frequency offset with quadratic and cubic power functions, as opposed to logarithmic functions, is greatly improved in the range dimension [17]. Random frequency offset has been used to achieve low beam sidelobes [18], but it is complex to implement. A symmetrical multicarrier FDA based on convex optimization was proposed [19] and shown to be capable of forming a dot-shaped beampattern and improving the performance of energy focusing and sidelobe suppression. The beampattern performance produced by using the new functional frequency offset obtained by combining natural logarithm and sine functions [20] and by using the Hamming window function frequency offset proposed in [21] is better than that produced by using logarithmic frequency offset and other functional frequency offsets. Methods such as symmetric logarithmic frequency offset [22], discrete Fourier transform [23], and Taylor windowing [24] also perform well in suppressing sidelobes in the range domain and angle domain, resulting in superior dot-shaped beampatterns. To suppress interference of the FDA beampattern, FDA is combined with the multiple-input multiple-output (MIMO) system, and simulated results verified the ability of FDA-MIMO to suppress interference in different scenarios [25]. The focus beam synthesis method based on the genetic algorithm, proposed in [26] to optimize the frequency offset increment, can synthesize single-point and multipoint transmission beams, and can also suppress sidelobes. FDA can also use adaptive [27], multibeam [28], broadband applications [29], and reconfigurable [30] thinned array methods to reduce sidelobe levels and reduce interference.

Because of its single linear structure, a conventional FDA has certain angle limitations in beam scanning. Under extreme angle conditions, the antenna gain will decrease [31], and the mainlobe beam will widen, which is not beneficial to target monitoring. For application scenarios that require the antenna to scan in all directions in various fields, the antenna needs to produce a narrower mainlobe beam with a lower sidelobe level [32]. In this case, circular array geometry is valuable for antenna beamforming. A frequency diverse arc array (FDAA) is proposed to achieve the wide beam scanning capacity. It is capable of 360-degree omni-directional beam scanning because it selectively activates array elements, utilizes precise phase compensation, and has special symmetrical logarithmic frequency offset. FDAA consists of antenna array elements with a uniform angular distribution on an arc-shaped structure. On the basis of FDA beam scanning, the array elements on the arc are activated circularly, so FDAA can flexibly manipulate the azimuth angle of the beam scanning. Furthermore, FDAA imposes an additional frequency offset on each operating array element and provides a method for controlling the beampattern in the target range domain and angle domain. Therefore, FDAA can monitor the selected target area in all directions covering 360 degrees, leading to more accurate and reliable locking of the target area.

By taking advantage of the arc structure, FDAA performs beam scanning through selectively activating operating array elements, but it has the problem of excessive beam spacing, and, thus, excessive beam granularity, leading to failure to meet the needs of certain scenarios [33]. To minimize the losses of antenna gain and power transmission, in this study, we propose a new beam scanning method for FDAA based on virtual array elements. This method can set a virtual reference at any position within the antenna aperture, and, based on the virtual array element, flexibly perform beam scanning through phase shifting on the equiphase surface, thereby reducing the span of beam pointing. This method effectively avoids the loss of antenna gain during scanning. To reduce the effects of inverse density weighting of FDAA, we obtain a better dot-shaped beampattern by optimizing amplitude weighting.

2. Structure Model of FDAA

The FDAA adopts open horn-shaped directional array elements that integrate transmitting. As shown in Figure 1, a series of antenna elements are evenly arranged along the arc to form an FDAA. The total number of array elements inside the entire arc is N, the array radius is R, the angular spacing between adjacent array elements on the arc is d_c, and the angular distance between adjacent array elements on the arc is $\Delta\phi$. The aperture angle formed by the operating elements selected and activated is ϕ.

Similar to a linear aperture synthesized by multiple array elements in a conventional FDA [34], the FDAA is also composed of multiple array elements. However, each array element of the FDAA is located outside the circular arc structure surface and is selected as an operating array element through feed activation, and then beampattern synthesis is achieved by configuring the phase.

To analyze the structure of FDAA more thoroughly, as shown in Figure 2, Take the true north direction of the 0th element f_0 as the reference direction. The angle θ of the target P of the far-field is the angle between the target direction and north. The range of θ is $[0, 360^\circ)$, and the N array elements along the arc are numbered clockwise. Aperture angleformed ϕ includes activated array elements such as $f_{-M}, \ldots, f_{-1}, f_0, f_1, \ldots, f_M$, and the frequency of the 0th array element is f_c, and each working array element is symmetrically arranged on both sides. In addition, an additional frequency offset is included between the array elements. The method for selecting the array element as the reference array element is expressed by:

$$f_0 = \text{round}\left(\frac{\theta}{\Delta\phi}\right) = \text{round}\left(\frac{\theta}{360/N}\right) \tag{1}$$

where round$(\cdot)$ represents the rounding operation and $\Delta\phi$ represents the angle between adjacent array elements, which can also be referred to as beam granularity. In the work of FDAA, expected signals, interference signals, and noise from different directions will be received at the same time. The core task of the system processing is to reduce the interference and noise effect of the desired target signal energy to the greatest advantage. When the total number of array elements is small, the array element spacing will be large, and there will be a large error in selecting the reference array element, which is not conducive to antenna beam scanning. Therefore, increasing the number of array elements appropriately can reduce the array element spacing and correct the phase error between array elements.

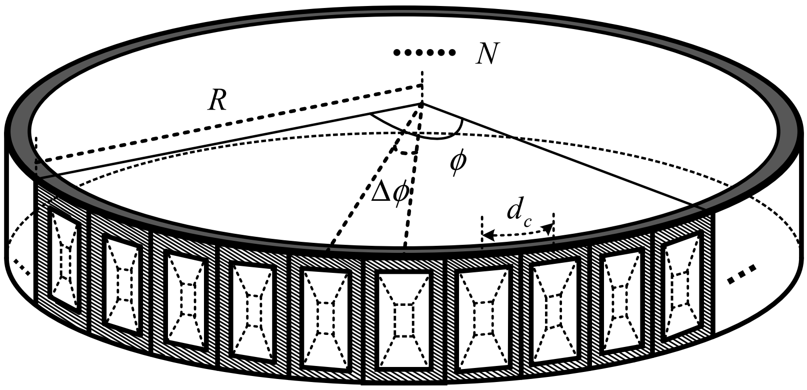

Figure 1. Three-dimensional geometric structure of FDAA.

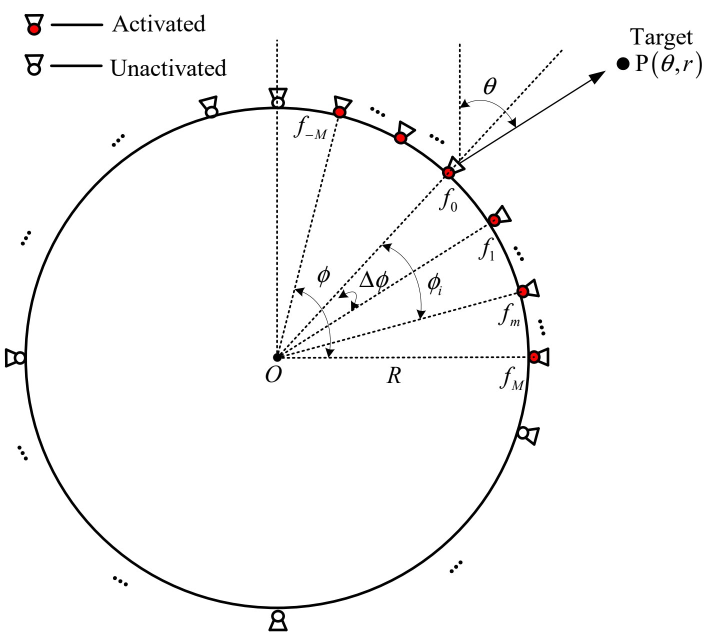

Figure 2. Two-dimensional geometric structure of FDAA.

3. FDAA Beampattern Synthesis and Optimization Method Based on Virtual Array Element

Through the introduction of the FDAA structure in the second section, we can see that, due to wide array element spacing, errors occur in selecting the reference array element for the target. Therefore, in this section, an FDAA beampattern synthesis and optimization method based the virtual array element is proposed. The specific process is described in Figure 3. First, the virtual array element is determined as the reference array element. Then, operating array elements are selected and activated. Next, the phase compensation and frequency design are performed in order to form an equiphase surface. Finally, the beampattern synthesis and optimization are completed.

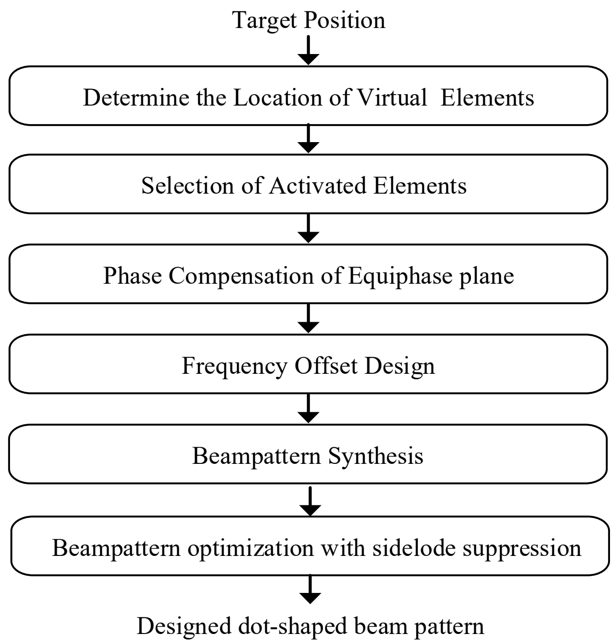

Figure 3. The flow diagram of the proposed method.

The beam granularity $\Delta\phi$ should be selected based on the radar system. It is limited by the array element spacing of the array antenna, and it is related to the total number of elements N of FDAA, generally the half-power beam width. The selection of the array element spacing should avoid the occurrence of grating lobes. If the coupled wave voltages of the array elements tend to be additive in phase, a large reflection can occur, thereby forming an observation blind area. Usually, to avoid serious mismatching of the array elements near the grating lobes, measures such as the residual method or wide-angle matching should be taken.

3.1. Setup of Virtual Array Element and Activation Method of Operating Array Element

As shown in Figure 4, the angle θ between the selected direction and north, measured clockwise, is the beam pointing direction, i.e., the desired target pointing direction of the beam. The position of the intersection between the desired pointing line and the arc front is the position of the virtual array element. When the total number of array elements is large enough, the position of the selected virtual array element is approximately in the middle position of adjacent array elements. Then the central angle of the m-th array element relative to the virtual array element is:

$$\phi_m = \begin{cases} \phi_{1,\ldots,M} = (m-0.5)\cdot\Delta\phi \\ \phi_0 = 0 \\ \phi_{-M,\ldots,-1} = (m+0.5)\cdot\Delta\phi \end{cases} \quad (2)$$

where $m = -M, \ldots, 0, \ldots, M$.

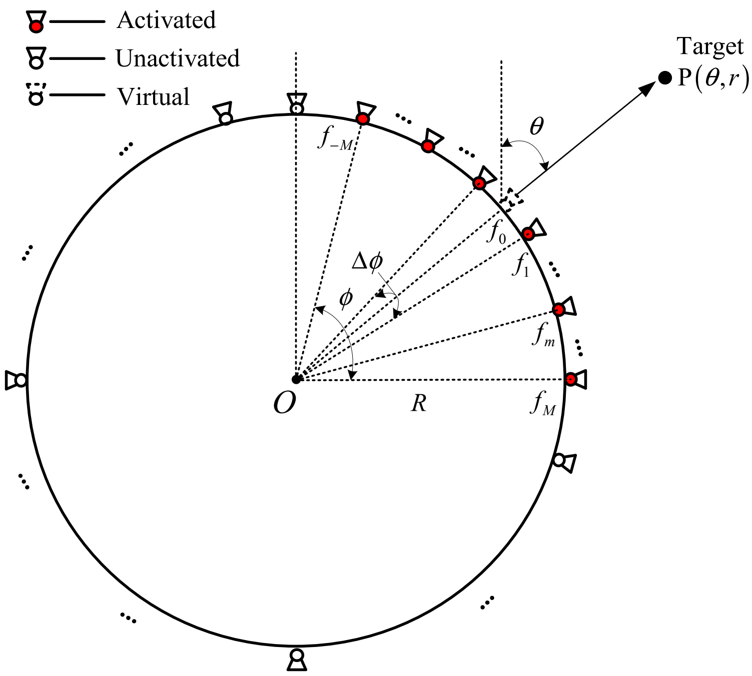

Figure 4. Beam scanning based on virtual element.

With the position of the virtual array element defined, due to the nonlinear distribution of the spatial phase difference caused by the special curvature of the FDAA, a single array element can only contribute to the gain of the main beam of the array in a certain area. Thus, at different scanning angles, it is necessary to activate appropriate array elements to form an operating array, and to use the feed system to selectively activate the operating array elements accordingly. The relationship between the horizontal length L of the operating array composed of activated array elements and the maximum beamwidth θ_{BW} of the far-field target P in the angle domain is expressed as:

$$L = k \cdot \frac{\lambda}{\theta_{BW}} \tag{3}$$

where k is the 3 dB beamwidth coefficient, which is usually in the range of $(0.88, 1.2)$, and λ is the wavelength [31]. The three-dimensional structure of the FDAA antenna is shown in Figure 5. The horizontal length of the active array elements forming the operating array can be expressed as:

$$L = 2R\sin(\phi/2) \tag{4}$$

The value of L is related to the angle between adjacent elements, from which the aperture angle of the activated array element is obtained as:

$$\phi = 2\arcsin(\frac{kc}{2Rf_c\theta_{BW}}) \tag{5}$$

where c is the speed of light and f_c is the carrier frequency. According to the geometry of the arc structure, the total number of activated array elements can be expressed as:

$$N_A = 2 \cdot \left\lfloor \frac{\phi}{2 \cdot \Delta\phi} \right\rfloor + 1 \tag{6}$$

where $\lfloor \cdot \rfloor$ represents the rounding operation. As shown in Figure 1, $N_A = 2M + 1$, so N_A is an odd number.

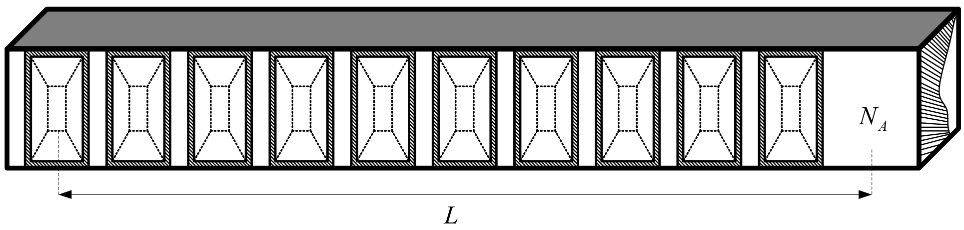

Figure 5. FDAA activated elements expansion diagram.

With the virtual array element as the reference, the activated operating array elements are renumbered on both sides. The elements along the arc are numbered $1, \ldots, M$ in the clockwise direction, and the elements along the arc are numbered $-1, \ldots, -M$ in the counter-clockwise direction.

3.2. Phase Compensation

As shown in Figure 6, with the defined operating array elements, there is a phase difference between each array element and the virtual array element. Thus, phase compensation is required to allow for scanning on the equiphase surface. Using the corresponding spatial phase difference obtained from the spatial travel difference in the operating array elements, spatial phase compensation between the operating array elements and the virtual array element is made, achieving the formation of the equiphasic surface. As shown in Figure 6, the spatial distance between an operating array element and the virtual array element can be expressed as:

$$D_m = 2R\sin^2(\phi_m/2) \tag{7}$$

On the equiphase surface formed based on the spatial distance, the required phase compensation of the operating array element relative to the virtual array element is:

$$\Delta\varphi_m = \frac{2\pi f_c}{c} \cdot D_m \tag{8}$$

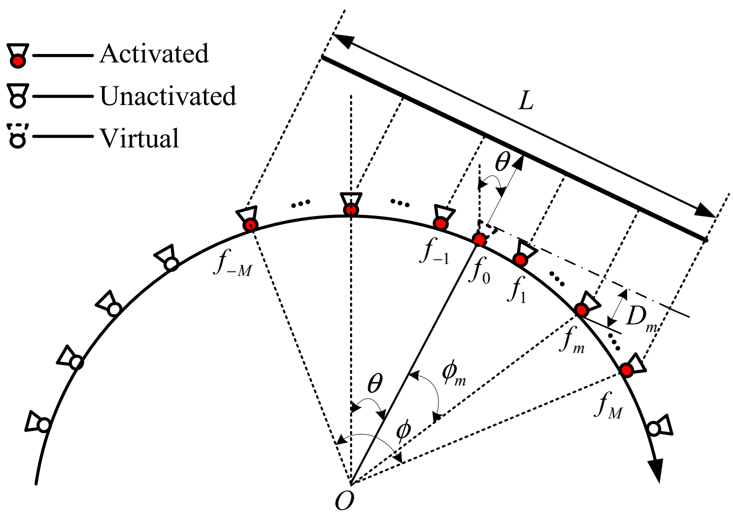

Figure 6. Phase compensation diagram of FDAA based on virtual the element.

3.3. Design of Frequency Offset

Affected by the structure of FDAA, special frequency offsets are designed according to the position of the virtual array element to obtain a single maximum beampattern with precise focusing. Suppose that the length L of a conventional linear FDA is the same as that of the proposed FDAA, and both are symmetrical arrays. The distance between the m-th array element in the linear FDA and the reference array element, x_{lm}, and the distance between the m-th array element and the reference array element on the equiphase surface of the FDAA, x_{cm}, can be respectively expressed as:

$$x_{cm} = R\sin\phi_m \tag{9}$$

$$x_{lm} = |m| \cdot \frac{2R\sin(\phi/2)}{M} \tag{10}$$

Thus, the distribution coefficient of the m-th array element in FDAA is:

$$\beta(m) = \frac{x_{cm}}{x_{lm}} = \frac{M}{2\sin(\phi/2)} \cdot \frac{\sin\phi_m}{|m|} \tag{11}$$

With the increase in array elements, the distribution coefficient presents a trend of first increasing and then decreasing, which is consistent with the characteristic of "sparse in the middle and dense on both sides" of FDAA formed by inverse density weighting.

The equiphase surface shown in Figure 7 is not uniform in terms of spacing. The equiphase surface consists of m activated operating array elements. The carrier frequency is f_c. Using f_0 of the reference array element as the reference point, the frequency of the transmitted signal of the m-th array element is designed as:

$$f_m = f_c + \Delta f_m \tag{12}$$

where Δf_m is the frequency offset of the m-th array element, which can be chosen to be Δf_{m1} or Δf_{m2}:

$$\Delta f_{m1} = \Delta f \cdot \ln(\beta(m) \cdot m + 1) \tag{13}$$

$$\Delta f_{m2} = \Delta f \cdot \left(0.54 - 0.46\cos(\frac{2\pi\beta(m) \cdot m}{2M})\right) \tag{14}$$

where Δf is a fixed frequency offset, and f_{m1} is a frequency offset based on symmetric logarithm. According to the array structure of the equiphase plane of FDAA, the removal of range-angle coupling can be accomplished by using logarithmic frequency offset distributed symmetrically on both sides. In addition, f_{m2} is a frequency offset based on a cosine window function. Compared with Hamming frequency offset, Hamming frequency offset has better performance in reducing amplitude of the sidelobes. The effectiveness of the two frequency offsets is compared to determine the best frequency offset.

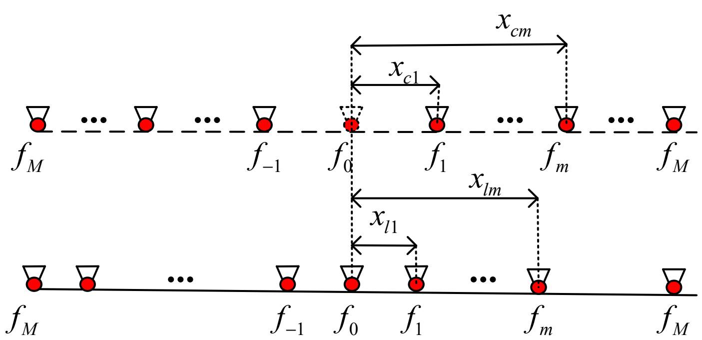

Figure 7. Comparison of equiphase plane based on virtual element and traditional FDA.

3.4. Beampattern Synthesis

As shown in Figure 8, assuming that the target under monitoring satisfies the far-field approximation condition at any place, the target is at point P. According to FDA antenna fundamentals [2], the signal emitted by the m-th array element can be expressed as:

$$X_m(t) = A_m \exp(j2\pi f_m t), 0 < t < T \tag{15}$$

where A_m represents the complex weight of the m-th array element and T represents the pulse duration of the transmission. The distance between the m-th array element and the target point should be:

$$r_m = r - x_{cm} \sin\theta \approx r - R\sin\phi_m \sin\theta \tag{16}$$

where r is the distance from the target, θ is the direction of the target, as well as $f_c \gg \Delta f_m$ and $r \gg R\sin\phi_m \sin\theta$. Then the total signal at the far-field target under monitoring P is:

$$\begin{aligned} X(t,r,\theta) &= \sum_{-M}^{M} X_m\left(t - \tfrac{r_m}{c}\right) \\ &= \sum_{-M}^{M} A_m \exp\left\{j2\pi(f_c + \Delta f_m)\left(t - \tfrac{r - R\sin\phi_m \sin\theta}{c}\right)\right\} \\ &\approx \exp\left[j2\pi f_c\left(t - \tfrac{r}{c}\right)\right] \sum_{-M}^{M} A_m \exp\left[j2\pi \ln(\beta(m)\cdot|m| + 1)\Delta f\left(t - \tfrac{r}{c}\right)\right] \\ &\times \exp\left(j2\pi f_c \tfrac{R\sin\phi_m \sin\theta}{c}\right) \end{aligned} \tag{17}$$

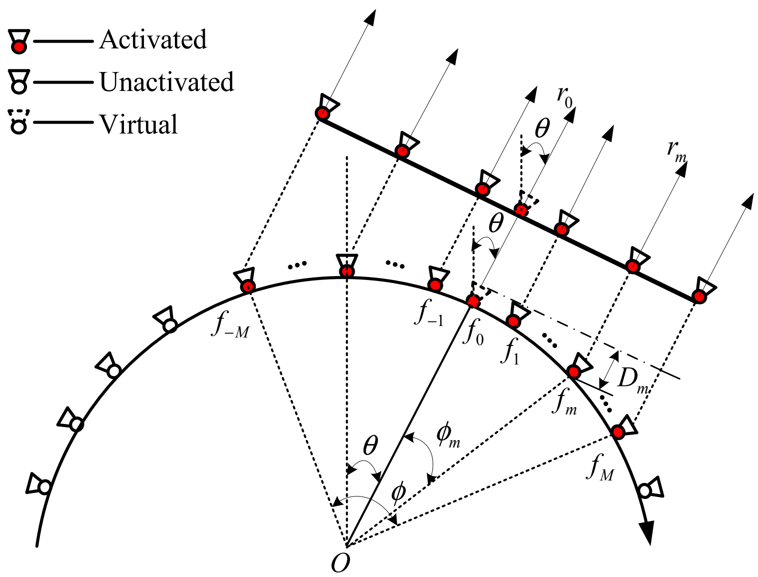

Figure 8. FDAA beampattern synthesis diagram based on virtual element.

Therefore, the array factor of FDAA can be expressed as:

$$\begin{aligned} \mathrm{AF}(t,r,\theta) &= \sum_{-M}^{M} A_m \exp\left[j2\pi\Delta f \cdot \ln(|\beta(m)\cdot m| + 1)\cdot\left(t - \tfrac{r}{c}\right)\right]\cdot \\ &\exp\left(j\cdot 2\pi f_c \tfrac{x_{cm}\sin\theta}{c}\right) \end{aligned} \tag{18}$$

In order for the target under monitoring to have a single peak at the desired range and azimuth (r_0, θ_0), the complex weight A_m can be calculated as:

$$A_m = \exp\left\{j\left[\frac{2\pi\Delta f_m r_0}{c} - \frac{2\pi f_c x_{cm}\sin\theta_0}{c} - \Delta\varphi_m\right]\right\} \tag{19}$$

Then the beampattern at the expected target can be expressed as:

$$\begin{aligned} B(t,r_0,\theta_0) = &\left|\sum_{M}^{-M} \exp\left[j2\pi\left(t - \tfrac{r - r_0}{c}\right)\cdot\Delta f\cdot\ln(|\beta(m)\cdot m| + 1)\right]\right. \\ &\times \left.\exp\left[j2\pi f_c \tfrac{R\sin\phi_m(\sin\theta - \sin\theta_0) - 2R\sin^2(\phi_m/2)}{c}\right]\right| \end{aligned} \tag{20}$$

3.5. Sidelobe Suppression

As shown in Figure 9, due to the special, arc-shaped surface structure of FDAA, after the formation of the equiphase surface, the spacing of operating array elements is sparse in the middle and dense on both sides. This phenomenon, called inverse density weighting, leads to high sidelobes of the antenna pattern, which is not conducive to the beam concentration at the target. The impact of this phenomenon can be clearly seen in Figure 10.

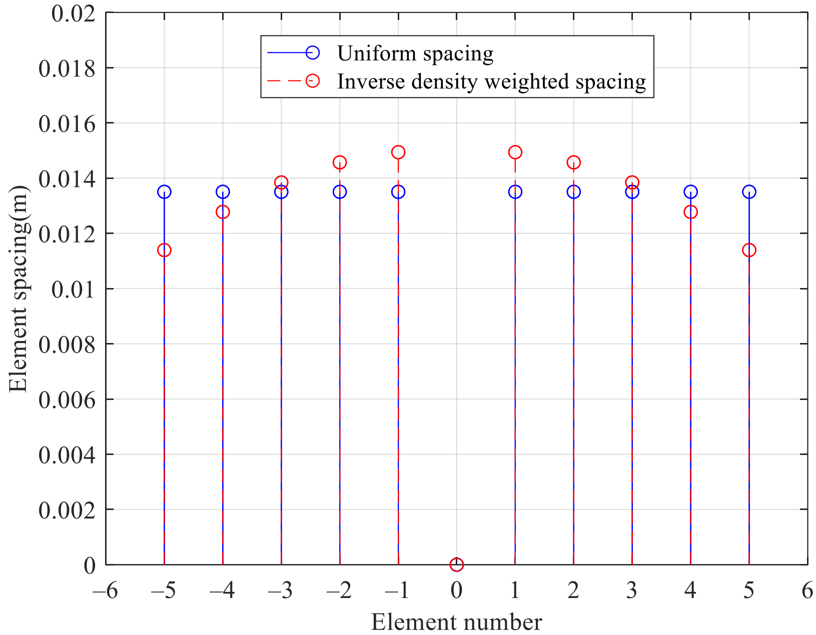

Figure 9. Element spacing for each element.

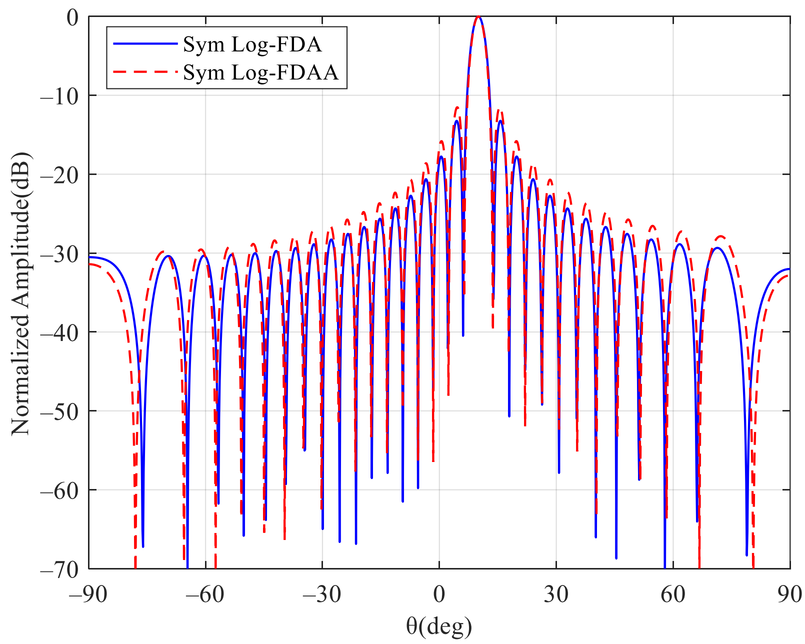

Figure 10. Comparison of FDA and FDAA.

The purpose of amplitude weighting is to quantify excitation amplitudes of the array elements in the array under the condition of uniform excitation of the antenna, and then to improve the sidelobe level of the antenna. The quality of weighting with a window function has a key effect on the beam performance. To reduce the problem of high sidelobes caused by inverse density weighting and to make the beam more concentrated at the target, we use two window functions, Hamming and Taylor windowing, which are suitable for non-uniform arrays, to optimize the amplitude weighting.

The Hamming window function is a special cosine window function [21]. Compared with the Hamming window, it can attenuate the sidelobe more. The Hamming window function can be expressed as:

$$w_1(n) = 0.54 - 0.46 \cdot \cos\left(\frac{2\pi n}{2M}\right), -M \le n \le M \tag{21}$$

The peak sidelobes generated by the Taylor window function [24] and the Hamming window function are relatively close, so the two functions have similar performance. In addition, the sidelobes far away from the main lobe are gradually attenuated. The Taylor window function is expressed as

$$w_2(n) = 1 + 2\sum_{a=-M}^{M} F_a \cdot \cos\left(\frac{2\pi X(n)a}{2N_A}\right) \tag{22}$$

Its related coefficients can be calculated using:

$$F_a = \frac{(-1)^{a+1}\prod_{k=-M}^{M}\left(1 - \frac{\frac{a^2}{\sigma^2}}{A^2+(k-0.5)^2}\right)}{2\prod_{j=-M}^{M}\left(1 - \frac{a^2}{j^2}\right)}, -M \le a \le M \tag{23}$$

$$\sigma^2 = \frac{{N_A}^2}{A^2 + (N_A - 0.5)^2} \tag{24}$$

with

$$A = \frac{\ln(B + \sqrt{B^2 - 1})}{\pi} \tag{25}$$

$$B = 10^{-\frac{S}{20}} \tag{26}$$

It should be noted that S is an optimizable negative number; $S = -51$ is used for the calculation.

4. Comparative Analysis of Simulation Results

4.1. Analysis of Simulation Results before Optimization

The sidelobe levels fundamentally reflect the strength of the space array antenna's ability to suppress the interference signal sources. The sidelobe interference signal power can be reduced as much as possible under the premise of maintaining the power of the target signal. In an array antenna, sidelobe performance is closely related to tactical and technical radar parameters. The two performance parameters, 3 dB main lobe band width (BW) and peak sidelobe level (PSLL), play a deciding role in the anti-clutter interference ability of the whole system.

According to the density weighting theory of a phased array antenna, density weighting is the design of antenna array elements with non-equal spacing, which can achieve the sidelobe level reduced by amplitude weighting and simplify the feeder grid design without losing the transmitted power. However, the resolution of FDAA array is affected by the arcuate structure, which forms a fixed non-uniform array of "sparse in the middle and dense on both sides" after the equiphase plane, which is just the opposite of the density-weighted optimization method.

In the simulation experiment, the parameters shown in Table 1 are used. Figure 11a–c corresponds to a conventional FDA based on symmetric logarithmic frequency offset.

Figures 11d–f and 11g–i present the simulation results at two symmetrical and non-uniform frequency offsets of f_{m1} and f_{m2}, both forming a single dot-shaped beam, and removing the range-angle coupling of the FDAA. However, we can see the effect caused by FDAA inverse density weighting and the more noticeable interference around the dot-shaped beam at the target. In contrast, FDAA performs better at f_{m1}, which will be optimized by amplitude weighting, described in the next subsection.

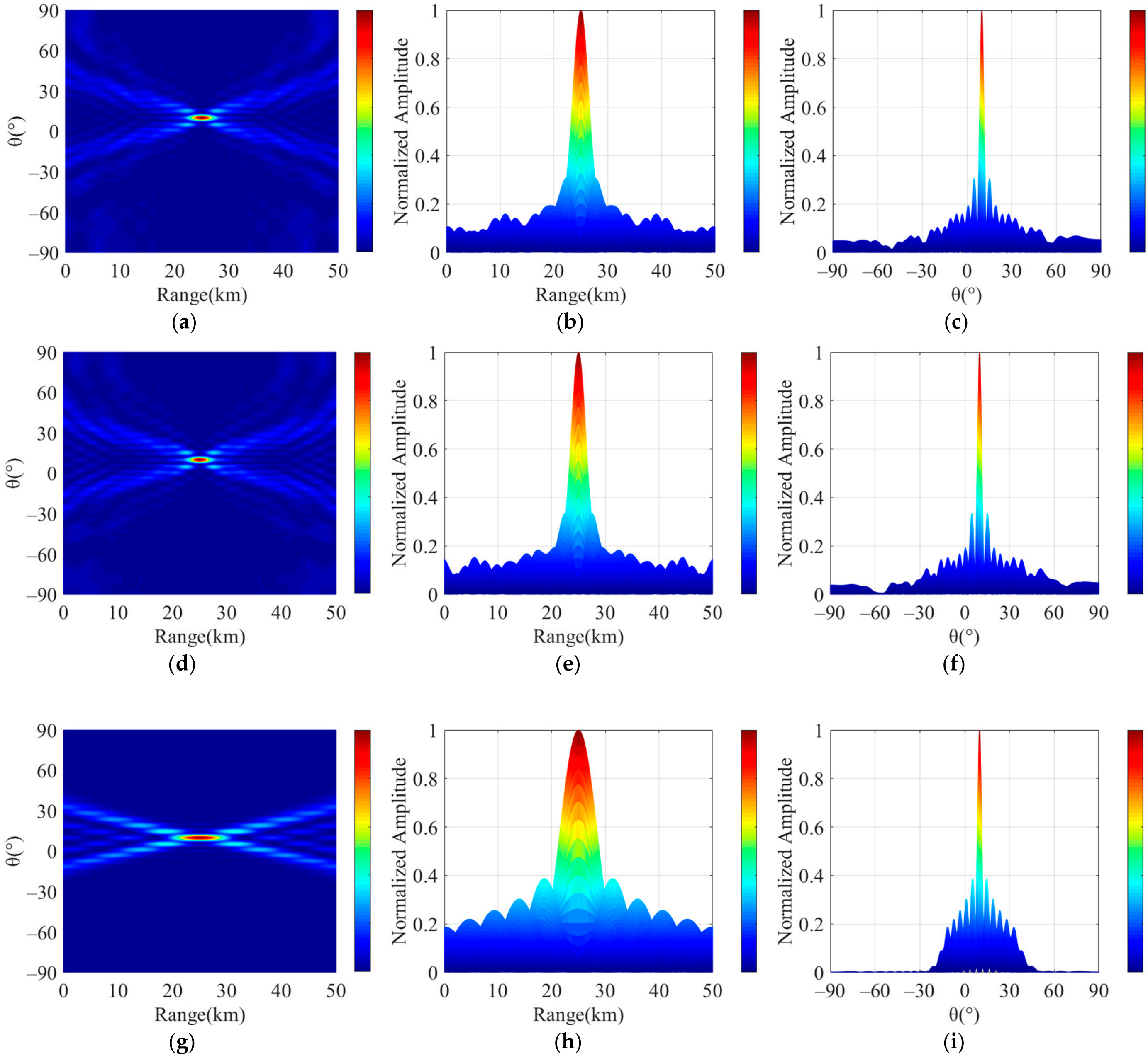

Figure 11. Beampattern synthesis results before optimization. (**a**) Sym Log-FDA. (**b**) Sym Log-FDA in the range domain. (**c**) Sym Log-FDA in the angle domain. (**d**) Sym Log-FDAA. (**e**) Sym Log-FDAA in the range domain. (**f**) Sym Log-FDAA in the angle domain. (**g**) Sym Hamming-FDAA. (**h**) Sym Hamming-FDAA in the range domain. (**i**) Sym Hamming-FDAA in the angle domain.

Table 1. Simulation parameters.

Parameters	Symbol	Value
Carrier frequency	f_c	10 GHz
Frequency offset	Δf	30 kHz
Element number	N_A	33
Element spacing	d_c	0.015 m
Array radius	R	0.3056 m
Array radian	ϕ	$\pi/2$
Desired target range	r_0	25 km
Desired target angle	θ_0	10°

4.2. Analysis of Simulation Result after Optimization

As shown in Figure 12a–c, in the beampattern after Hamming window amplitude weighting in the FDAA, the dot-shaped beam optimization effectiveness is quite noticeable, the first-order sidelobe in the range domain is greatly suppressed, and the sidelobe levels around the main lobe in the range domain are significantly reduced. Compared with the angle domain before optimization, the overall sidelobe level is reduced, and the removal of sharp peaks is noticeable. As shown in Figure 12d–f, the dot-shaped beampattern after the Taylor window amplitude weighting is very similar to that with the Hamming window amplitude weighting. Additionally, the sidelobe level distribution in the range domain is smoother, which is beneficial to the engineering implementation. The main lobe beam is narrower in the angle domain, but the level of the first order sidelobe is slightly higher.

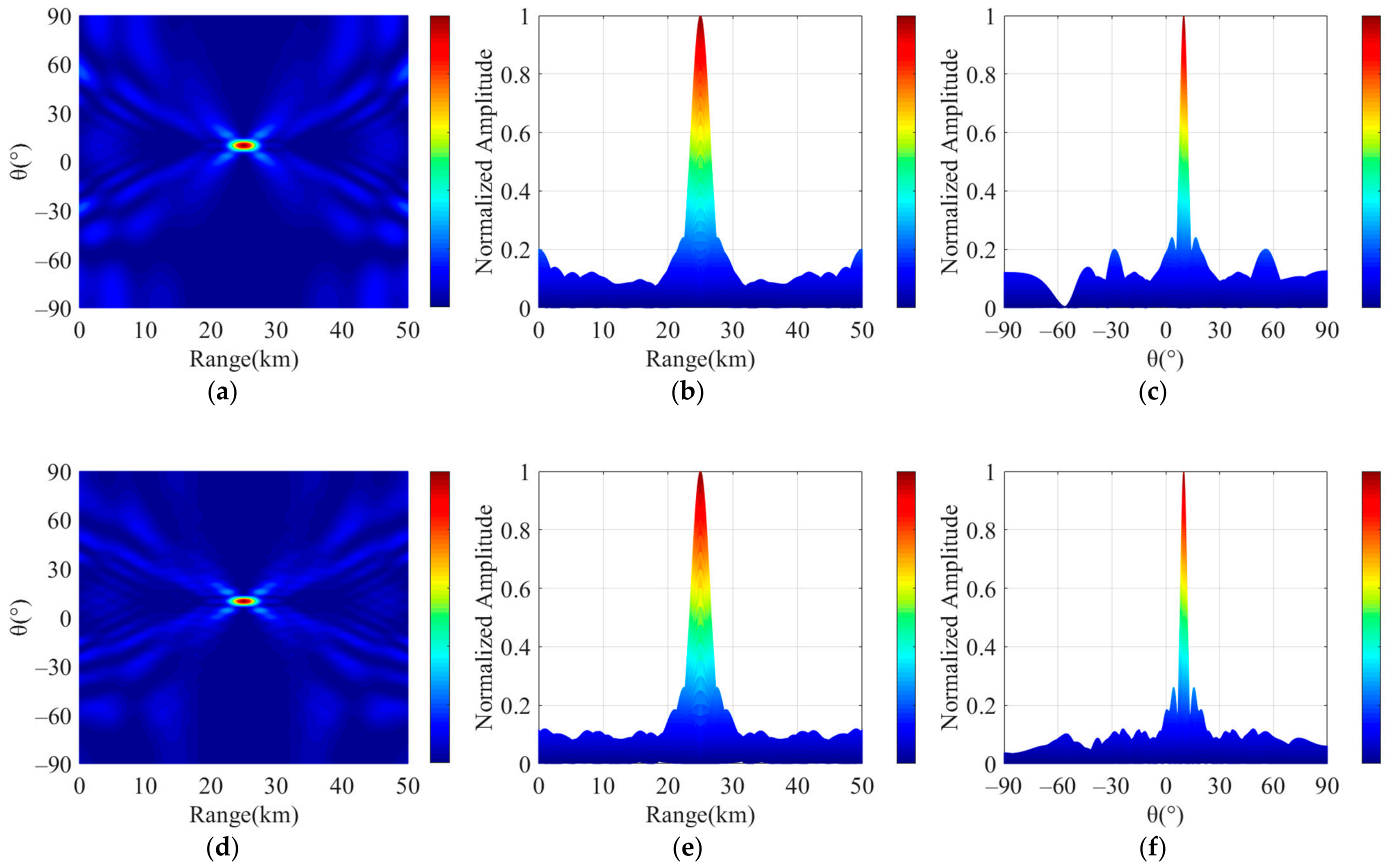

Figure 12. Beampattern synthesis results after optimization. (**a**) Hamming weighted Sym Log-FDAA. (**b**) Hamming weighted Sym Log-FDAA in the range domain. (**c**) Hamming weighted Sym Log-FDAA in the angle domain. (**d**) Taylor weighted Sym Log-FDAA. (**e**) Taylor weighted Sym Log-FDAA in the range domain. (**f**) Taylor weighted Sym Log-FDAA in the angle domain.

Finally, the patterns of array antennas are compared concisely. In the range domain shown in Figure 13, it can be seen that, after optimization, the width of the main lobe is reduced, the sidelobes are narrowed, and the interference suppression and focusing effectiveness are significantly improved. From the angle domain in Figure 14, it can be seen that with the Hamming window amplitude weighting, the sidelobe is reduced greatly and the main lobe is widened; with the Taylor window amplitude weighting, the sidelobe is reduced to a lesser extent, and the main lobe is widened to a lesser extent. Compared with before optimization, after using Hamming and Taylor window functions for amplitude weighting optimization, the sidelobe suppression of the FDAA antenna pattern is remarkable, reducing the impact of inverse density weighting.

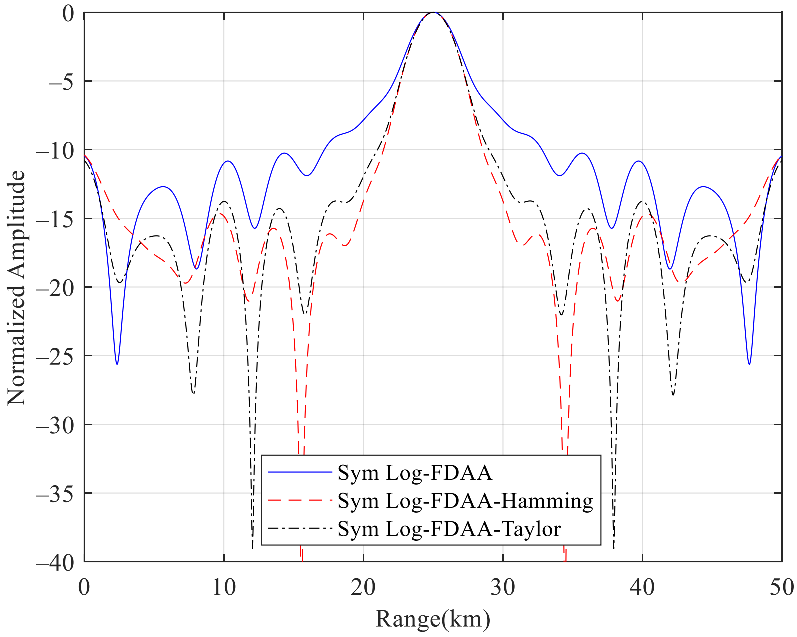

Figure 13. Comparison of beampattern in range dimension before and after optimization.

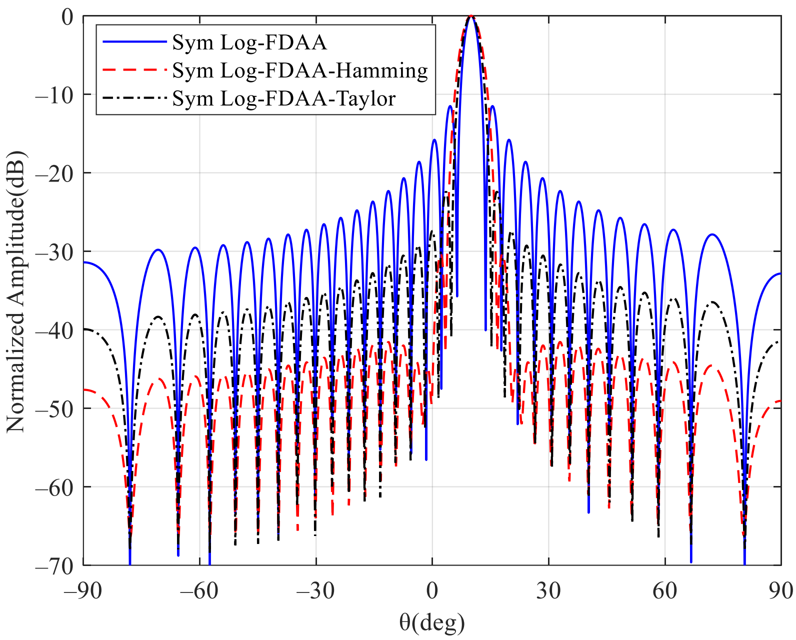

Figure 14. Comparison of beampattern in angle dimension before and after optimization.

5. Conclusions

In this paper, FDAA is shown to have the problem of inverse density weighting on the equiphase surface of each operating array element. This leads to high sidelobe level, causing interference to the dot-shaped beampattern for target monitoring. To tackle this problem, we have proposed a beampattern synthesis and optimization method for FDAA based on virtual array elements. This method performs beampattern synthesis by setting up the position of the virtual array element, configuring the phase compensation of the operating array elements, and designing special frequency offsets for FDAA beams, thereby reducing the beam granularity error between adjacent array elements. This method uses amplitude weighting to optimize the beam, which greatly reduces the effect of inverse density weighting on the beam, and effectively solves the interference of sidelobes on the target. This method yields a superior dot-shaped beampattern and peak-to-sidelobe ratio. As a result, it improves radar antenna measurement accuracy and resolution. FDAA, a new type of structural array antenna, achieves 360-degree omni-directional beam scanning by selectively activating array elements and implementing precise phase compensation, so it provides a new idea for radar, communication, and target monitoring in specific real-world scenarios. The feasibility and effectiveness of the method are verified by simulation results.

Author Contributions: Conceptualization, W.X.; methodology, W.X.; software, W.X. and Z.D.; validation, W.X. and P.H.; formal analysis, Z.D.; investigation, W.X. and Z.D.; resources, W.X., W.T. and Z.G.; data curation, Z.D.; writing—original draft preparation, W.X. and Z.D.; writing—review and editing, W.X. and P.H.; visualization, P.H.; supervision, W.T.; project administration, P.H. and W.T.; funding acquisition, W.X. and Z.G. All authors have read and agreed to the published version of the manuscript.

Funding: This research was supported by the National Natural Science Foundation of China under Grant Number 62071258, 61971246 and 52064039, in part by the Natural Science Foundation of Inner Mongolia, Grant Number 2020ZD18, and in part by the Key Project of Regional Innovation and Development Joint Fund of National Natural Science Foundation under Grant Number U22A2010.

Data Availability Statement: No applicable.

Conflicts of Interest: The authors declare no conflict of interest.

References

1. Antonik, P.; Wicks, M.C.; Griffiths, H.D.; Baker, C.J. Frequency diverse array radars. In Proceedings of the 2006 IEEE Conference on Radar, Verona, NY, USA, 24–27 April 2006.
2. Wang, W.-Q. Frequency Diverse Array Antenna: New Opportunities. *IEEE Antennas Propag. Mag.* **2015**, *57*, 145–152. [CrossRef]
3. Ivashina, M.V.; Maaskant, R.; Woestenburg, B. Equivalent System Representation to Model the Beam Sensitivity of Receiving Antenna Arrays. *IEEE Antennas Wirel. Propag. Lett.* **2008**, *7*, 733–737. [CrossRef]
4. Wang, W.Q. Range-Angle Dependent Transmit Beampattern Synthesis for Linear Frequency Diverse Arrays. *IEEE Trans. Antennas Propag.* **2013**, *61*, 4073–4081. [CrossRef]
5. Wang, Y.; Wang, W.Q.; Chen, H. Linear Frequency Diverse Array Manifold Geometry and Ambiguity Analysis. *IEEE Sens. J.* **2015**, *15*, 984–993. [CrossRef]
6. Liao, T.; Pan, Y.; Wang, W.Q. Generalized Linear Frequency Diverse Array Manifold Curve Analysis. *IEEE Signal Process. Lett.* **2018**, *25*, 768–772. [CrossRef]
7. Wang, S.B.L.; Xu, Z.H.; Liu, X.H.; Dong, W.; Wang, G.Y. A Novel Transmit-Receive System of Frequency Diverse Array Radar for Multitarget Localization. *Electronics* **2018**, *7*, 408. [CrossRef]
8. Wang, Y.; Zhu, S. Range Ambiguous Clutter Suppression for FDA-MIMO Forward Looking Airborne Radar Based on Main Lobe Correction. *IEEE Trans. Veh. Technol.* **2021**, *70*, 2032–2046. [CrossRef]
9. Gui, R.; Wang, W.-Q.; Farina, A.; So, H.C. FDA radar with doppler-spreading consideration: Mainlobe clutter suppression for blind-doppler target detection. *Signal Process.* **2021**, *179*, 107773. [CrossRef]
10. Ding, Z.; Xie, J. Joint Transmit and Receive Beamforming for Cognitive FDA-MIMO Radar with Moving Target. *IEEE Sens. J.* **2021**, *21*, 20878–20885. [CrossRef]
11. Han, X.; Ding, S.; Huang, Y.; Zhou, Y.; Tang, H.; Wang, B. Frequency Diversity Array for Near-Field Focusing. *Electronics* **2020**, *9*, 958. [CrossRef]
12. Ding, S.; Huang, Y.-M.; Tang, H.; Bozzi, M.; Wang, B.-Z. Achieving Spatial Multi-Point Focusing by Frequency Diversity Array. *Electronics* **2019**, *8*, 883. [CrossRef]
13. Ali, H.T.; Amin, S.; Amin, M.; Maqsood, M.; Maud, A.R.; Yusuf, M. Design and Development of a Near Isotropic Printed Arc Antenna for Direction of Arrival (DoA) Applications. *Electronics* **2021**, *10*, 797. [CrossRef]

14. Zhang, M.; Liao, G.; He, X.; Zhu, S. Unambiguous Forward-Looking SAR Imaging on HSV-R Using Frequency Diverse Array. *Sensors* **2020**, *20*, 1169. [CrossRef]
15. Wang, W.Q.; So, H.C.; Shao, H. Nonuniform Frequency Diverse Array for Range-Angle Imaging of Targets. *IEEE Sens. J.* **2014**, *14*, 2469–2476. [CrossRef]
16. Khan, W.; Qureshi, I.M.; Saeed, S. Frequency Diverse Array Radar with Logarithmically Increasing Frequency Offset. *IEEE Antennas Wirel. Propag. Lett.* **2015**, *14*, 499–502. [CrossRef]
17. Gao, K.; Wang, W.-Q.; Cai, J.; Xiong, J. Decoupled frequency diverse array range-angle-dependent beampattern synthesis using non-linearly increasing frequency offsets. *IET Microw. Antennas Propag.* **2016**, *10*, 880–884. [CrossRef]
18. Liu, Y.; Ruan, H.; Wang, L.; Nehorai, A. The Random Frequency Diverse Array: A New Antenna Structure for Uncoupled Direction-Range Indication in Active Sensing. *IEEE J. Sel. Top. Signal Process.* **2017**, *11*, 295–308. [CrossRef]
19. Shao, H.; Dai, J.; Xiong, J.; Chen, H.; Wang, W.Q. Dot-Shaped Range-Angle Beampattern Synthesis for Frequency Diverse Array. *IEEE Antennas Wirel. Propag. Lett.* **2016**, *15*, 1703–1706. [CrossRef]
20. Chen, B.; Chen, X.; Huang, Y.; Guan, J. Transmit Beampattern Synthesis for the FDA Radar. *IEEE Antennas Wirel. Propag. Lett.* **2018**, *17*, 98–101. [CrossRef]
21. Basit, A.; Qureshi, I.M.; Khan, W.; Rehman, S.u.; Khan, M.M. Beam Pattern Synthesis for an FDA Radar with Hamming Window-Based Nonuniform Frequency Offset. *IEEE Antennas Wirel. Propag. Lett.* **2017**, *16*, 2283–2286. [CrossRef]
22. Liao, Y.; Wang, W.Q.; Zheng, Z. Frequency Diverse Array Beampattern Synthesis Using Symmetrical Logarithmic Frequency Offsets for Target Indication. *IEEE Trans. Antennas Propag.* **2019**, *67*, 3505–3509. [CrossRef]
23. Zubair, M.; Ahmed, S.; Alouini, M.S. Frequency Diverse Array Radar: New Results and Discrete Fourier Transform Based Beampattern. *IEEE Trans. Signal Process.* **2020**, *68*, 2670–2681. [CrossRef]
24. Liao, Y.; Tang, H.; Chen, X.; Wang, W.Q. Frequency Diverse Array Beampattern Synthesis with Taylor Windowed Frequency Offsets. *IEEE Antennas Wirel. Propag. Lett.* **2020**, *19*, 1901–1905. [CrossRef]
25. Wang, W.Q.; So, H.C. Transmit Subaperturing for Range and Angle Estimation in Frequency Diverse Array Radar. *IEEE Trans. Signal Process.* **2014**, *62*, 2000–2011. [CrossRef]
26. Xiong, J.; Wang, W.Q.; Shao, H.; Chen, H. Frequency Diverse Array Transmit Beampattern Optimization with Genetic Algorithm. *IEEE Antennas Wirel. Propag. Lett.* **2017**, *16*, 469–472. [CrossRef]
27. Haupt, R.L. Adaptively thinned arrays. *IEEE Trans. Antennas Propag.* **2015**, *63*, 1626–1632. [CrossRef]
28. Buonanno, G.; Costanzo, S.; Solimene, R. Statistically Thinned Array Antennas for Simultaneous Multibeam Applications. *IEEE Access* **2022**, *10*, 60230–60240. [CrossRef]
29. Buonanno, G.; Costanzo, S.; Solimene, R. Broadband Statistically Designed Thinned-Binned Array Antennas. *IEEE Trans. Antennas Propag.* **2023**, *71*, 2454–2466. [CrossRef]
30. Haupt, R.L. Reconfigurable Thinned Arrays. In Proceedings of the 2014 IEEE Radar Conference, Cincinnati, OH, USA, 19–23 May 2014; pp. 76–78.
31. Xu, W.; Hu, J.; Huang, P.; Tan, W.; Dong, Y. Multiaperture Antenna Architecture Design for Azimuth Uniform Sampling in High-Resolution Wide-Swath SAR. *IEEE Antennas Wirel. Propag. Lett.* **2020**, *19*, 1042–1046. [CrossRef]
32. Lan, L.; Liao, G.; Xu, J.; Zhang, Y.; Fioranelli, F. Suppression Approach to Main-Beam Deceptive Jamming in FDA-MIMO Radar Using Nonhomogeneous Sample Detection. *IEEE Access* **2018**, *6*, 34582–34597. [CrossRef]
33. Lin, Y.; Hong, W.; Tan, W.; Wang, Y.; Xiang, M. Airborne circular SAR imaging: Results at P-band. In Proceedings of the 2012 IEEE International Geoscience and Remote Sensing Symposium, Munich, Germany, 22–27 July 2012; pp. 5594–5597.
34. Huang, P.; Tan, W.; Ying, S. MIMO-SAR imaging technology for helicopter-borne based on ARC antenna array. In Proceedings of the 2015 IEEE International Geoscience and Remote Sensing Symposium (IGARSS), Milan, Italy, 26–31 July 2015; pp. 1801–1804.